An *in vivo* multiplexed small-molecule screening platform

Barbara M Grüner[1,9], Christopher J Schulze[2,9], Dian Yang[3], Daisuke Ogasawara[4], Melissa M Dix[4], Zoë N Rogers[1], Chen-Hua Chuang[1], Christopher D McFarland[5], Shin-Heng Chiou[1], J Mark Brown[6], Benjamin F Cravatt[4], Matthew Bogyo[2,3,7,8] & Monte M Winslow[1–3,8]

Phenotype-based small-molecule screening is a powerful method to identify molecules that regulate cellular functions. However, such screens are generally performed *in vitro* under conditions that do not necessarily model complex physiological conditions or disease states. Here, we use molecular cell barcoding to enable direct *in vivo* phenotypic screening of small-molecule libraries. The multiplexed nature of this approach allows rapid *in vivo* analysis of hundreds to thousands of compounds. Using this platform, we screened >700 covalent inhibitors directed toward hydrolases for their effect on pancreatic cancer metastatic seeding. We identified multiple hits and confirmed the relevant target of one compound as the lipase ABHD6. Pharmacological and genetic studies confirmed the role of this enzyme as a regulator of metastatic fitness. Our results highlight the applicability of this multiplexed screening platform for investigating complex processes *in vivo*.

High-throughput phenotype-based small-molecule screens have contributed immensely to our understanding of many biological processes[1,2]. Using *in vivo* models for primary screening provides an opportunity to interrogate processes that cannot be accurately modeled *in vitro*. However, the application of small-molecule screening for the analysis of complex *in vivo* processes in higher vertebrates has been limited by the high cost- and effort-intensive nature of these studies, limited quantities of compounds in chemical libraries, and technical variability in group-to-group comparisons. Chemical screens in *Caenorhabditis elegans* and *Danio rerio* have identified modulators of several biological processes[3–5], and new technologies allow the efficacy of multiple chemotherapeutics to be tested simultaneously in tumors[6,7]. Nonetheless, large-scale *in vivo* chemical screens to investigate biological processes in higher vertebrates have not been possible.

To overcome these limitations, we established a methodology that allows the effect of hundreds of compounds to be assessed in parallel in an *in vivo* mouse model. We employed molecular barcoding combined with high-throughput sequencing to perform multiplexed analysis of compound pretreated cells. Molecular barcoding of cells has been used to track diverse subclones of cancer cells and hematopoietic stem cells *in vivo* as well as to monitor responses to chemotherapy *in vitro* and *in vivo*[8–13]. This technique is particularly suited to our screening approach as it allows quantification of differentially pretreated populations *in vivo*.

Pancreatic ductal adenocarcinoma (PDAC) is a malignancy that is almost uniformly fatal mainly because of its high rate of metastatic spread[14]. Despite insights into the genetics of pancreatic carcinogenesis, the molecular mechanisms enabling PDAC cells to leave the blood and enter a secondary organ—the initial steps of metastatic seeding—remain poorly understood[15–20]. Because of the challenges of *in vivo* analyses, most studies have focused on optimization of compounds with known targets[21] or *in vitro* assays to identify inhibitors of migration or invasion. While the latter approaches have become higher in throughput[22], *in vitro* assays likely fail to accurately recapitulate the entire *in vivo* process[23]. Here, we describe the development and initial application of a multiplexed screening platform that bridges the gap between high-throughput cell-based chemical screening and *in vivo* modeling of metastatic seeding.

RESULTS

Development of the multiplexed screening workflow

To allow multiplexed compound screening, we generated 96 uniquely barcoded isogenic variants of a pancreatic cancer cell line (**Fig. 1a** and **Supplementary Fig. 1**). These variants can each be pretreated with a single compound *in vitro*, pooled, injected intravenously into recipient mice, and isolated from the lungs after metastatic seeding. The lung represents one of the major metastatic sites for many cancer types including PDAC[18,24]. Determining the barcode representation by sequencing preinjection and postseeding samples allows parallel quantification of the
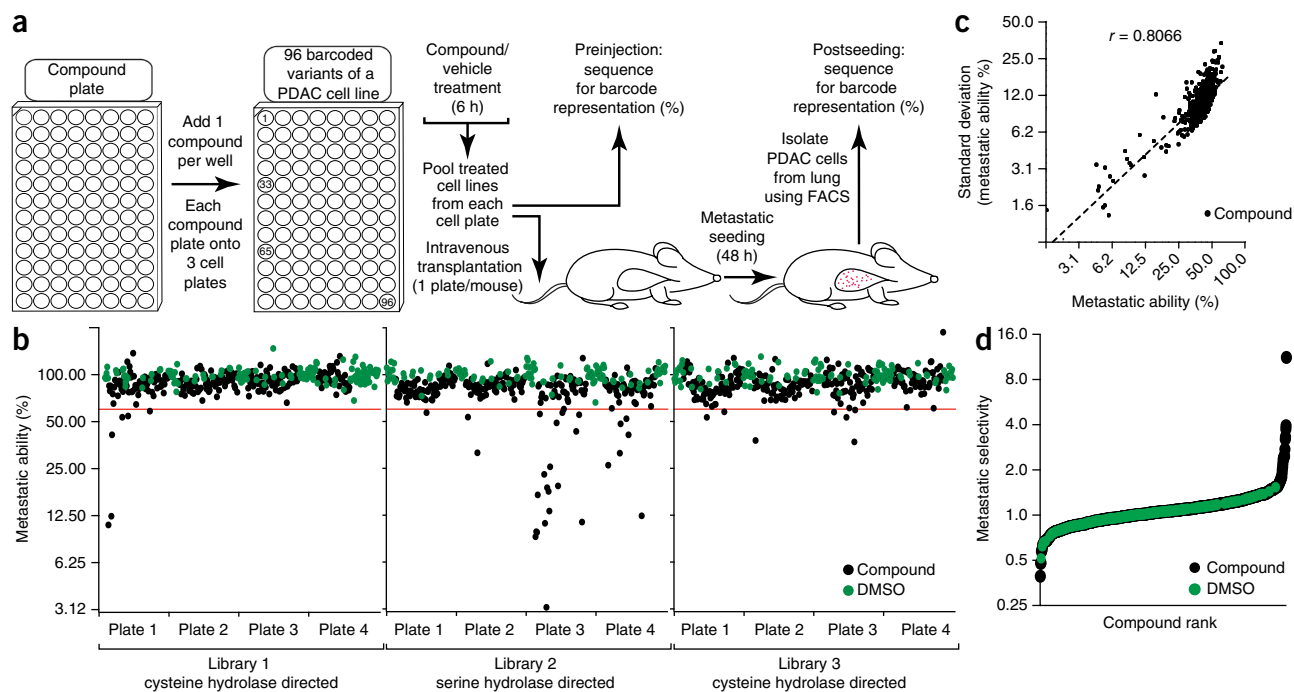
Figure 1 | Development and application of an *in vivo* multiplexed small-molecule screening platform to interrogate metastatic seeding. (**a**) Schematic of the multiplexed *in vivo* small-molecule screen. (**b**) Screening 712 small-molecule irreversible inhibitors at 10 µM distributed across 12 96-well plates. Each plate contained ≥26 DMSO wells as internal controls (green dots). All compound plates were tested in triplicate on three different barcode-layout plates. Each black dot represents the average loss of representation of one compound. The red line indicates a 40% loss of metastatic ability (~3× the s.d. of vehicle-treated control). (**c**) s.d. of the triplicate values for each compound is proportional to the metastatic ability for all screened compounds; *r* is the calculated Pearson correlation coefficient. The dotted line indicates the best-fit line. (**d**) Metastatic selectivity of the 712 compounds.

effect of each pretreatment on metastatic seeding ability (**Fig. 1a** and **Supplementary Fig. 2a,b**).

We chose a murine PDAC liver metastasis cell line (0688M) that was derived from the well-established $Kras^{LSL-G12D/+}$; $p53^{LSL-R172H/+}$;$Pdx1$-Cre;$Rosa26^{LSL-tdTomato/+}$ mouse model of human PDAC[25,26]. Among three tested cell lines, 0688M cells seeded the lung most efficiently and grew into macrometastases (**Supplementary Fig. 1a–c**). Using a Tomato$^+$ murine PDAC cell line allowed transplantation into immunocompetent mice, avoided potential cross-species incompatibilities, and enabled the isolation of cancer cells by fluorescence-activated cell sorting (FACS). We determined the optimal timepoint for postseeding analysis as 2 d after injection, when cancer cells in the lung have not yet begun to proliferate extensively, but cells that have not actively seeded have been cleared from the lung (**Supplementary Fig. 1d–f**).

Establishment of screen and parameters

To identify a hit threshold for selection of lead compounds, all 96 barcoded variants were treated with vehicle (DMSO), pooled, and assayed for their ability to seed the lungs of recipient mice. To generate the sequencing libraries from the DNA isolated from preinjection and postseeding samples, we PCR amplified the barcode region using primers containing multiplexing tags, Illumina adapters, and Illumina sequencing primer-binding sites. Samples amplified as technical replicates had high reproducibility (**Supplementary Fig. 3b,c**). The change in barcode representation was calculated between the postseeding and preinjection populations and compared to the average of all vehicle-treated samples

to define the 'metastatic ability' (%) of each treated cell population (**Supplementary Fig. 2b**). All barcoded cell lines showed similar metastatic ability, and triplicate assays had a s.d. of 13.5% (**Supplementary Fig. 3a**).

For the initial screen, we selected three focused libraries of compounds directed toward serine and cysteine hydrolases[27–29]. These hydrolase family enzymes include proteases, esterases, thioesterases, and lipases. The compounds all contain electrophilic traps that are designed to covalently bind their targets, enabling irreversible and sustained inhibition after *in vitro* pretreatment without the need for continued dosing. Furthermore, these compounds can be converted into activity-based probes (ABPs) for downstream target identification using proteomics.

Using the multiplexed screening platform, we assessed the antimetastatic effect of 712 compounds, including internal controls, in triplicate using only 36 mice (**Fig. 1b**). At the initial screening concentration of 10 µM, approximately 5% of the compounds (39) reduced metastatic ability *in vivo* below the threshold of 60%, and the assay exhibited well-behaved multiplicative errors with the s.d. proportional to the metastatic ability (Pearson's *r* = 0.81; **Fig. 1c**). To exclude cytotoxic compounds, we performed *in vitro* viability assays in parallel. We calculated the 'metastatic selectivity' for each compound as the fraction of loss of representation *in vivo* that is not attributable to reduced cell growth *in vitro* (**Fig. 1d**, **Supplementary Fig. 2b**, and **Supplementary Table 1**).

Hit prioritization and dose-dependent secondary screening

19 compounds were chosen for further dose–response studies (six concentrations from 10 µM to 0.31 µM) using metastatic
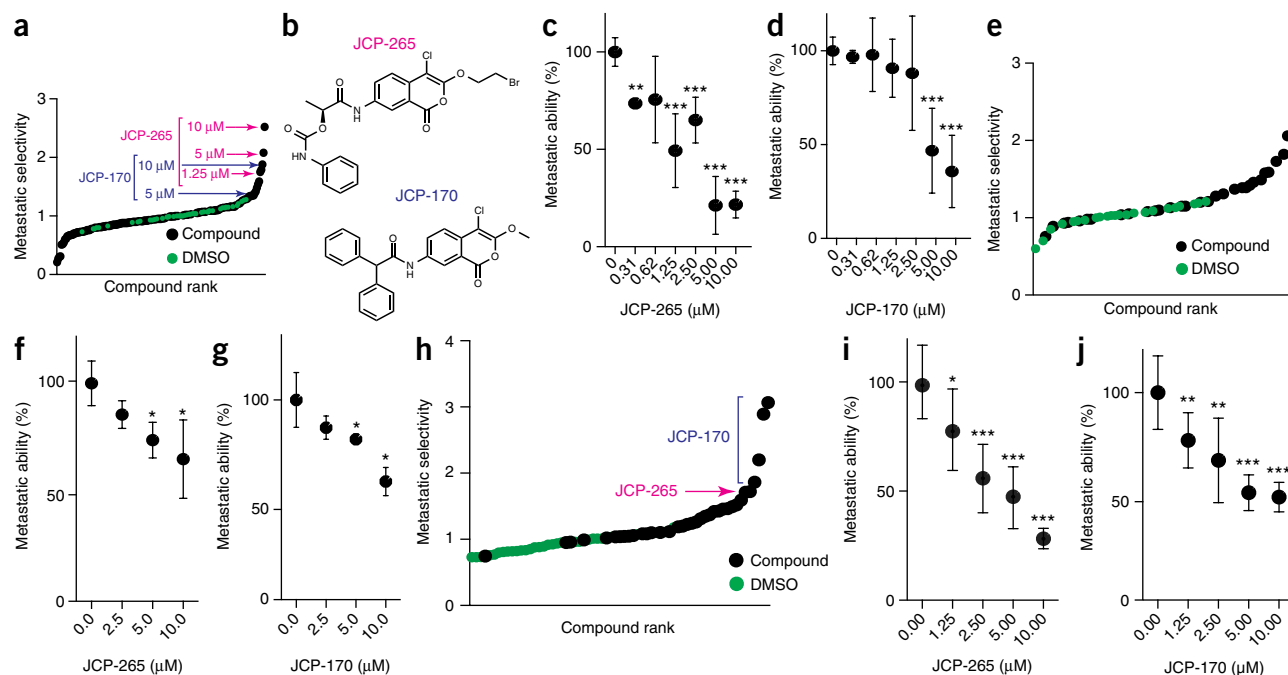
Figure 2 | *In vivo* dose–response screening in human and mouse PDAC cells for seeding to the lung and liver. (**a**) A multiplexed secondary screen for metastatic selectivity of 0688M cells treated with top hit compounds in dose–response. (**b**) Structures of JCP-265 and JCP-170. (**c**,**d**) Metastatic ability of 0688M cells treated with JCP-265 (**c**) or JCP-170 (**d**) within the secondary screen. $n = 3$ per concentration; $n = 25$ for control (0 μM); **$P < 0.01$; ***$P < 0.001$. (**e**) A multiplexed screen for metastatic selectivity of two human PDAC cell lines (AsPC-1 and Panc89) treated with the top hit compounds. (**f**,**g**) Metastatic ability of AsPC-1 human PDAC cells treated with JCP-265 (**f**) or JCP-170 (**g**) within the human cell lines screen. $n = 2$ per concentration, *$P < 0.05$. P values were calculated using the Mann–Whitney test; all dots represent the mean ± s.d. For dots that show no error bar, the error bar was smaller than the dot. (**h**) A multiplexed liver seeding screen for metastatic selectivity of 0688M cells treated with top hit compounds. (**i**,**j**) Metastatic ability of 0688M cells treated with JCP-265 (**i**) or JCP-170 (**j**) within the liver seeding screen. $n = 4$ per concentration; $n = 67$ for control (0 μM); *$P < 0.05$; **$P < 0.01$; ***$P < 0.001$. P values were calculated using the Mann–Whitney test; all dots represent the mean ± s.d.

selectivity, structural diversity, *in vitro* viability, and the magnitude of effect on *in vivo* metastatic ability as criteria for prioritization (**Supplementary Tables 1** and **2**). Our multiplexed screening strategy allowed the simultaneous analysis of multiple lead compounds at different concentrations *in vivo* in individual mice (**Supplementary Fig. 4a**). By performing parallel *in vitro* toxicity testing, we further prioritized five compounds with the most robust and selective antimetastatic effects (metastatic selectivity > 1.3, *in vitro* assays showing no significant effect on viability; **Fig. 2a** and **Supplementary Table 2**). A third independent multiplexed *in vivo* screen of the top compounds in a dose-dependent manner further confirmed the reproducibility of our screening platform (**Supplementary Fig. 4b–d** and **Supplementary Table 3**).

Screening human cells and metastatic seeding in the liver
Another important consideration in selecting lead compounds for target identification was their ability to reduce metastatic seeding of human PDAC cell lines. We generated uniquely barcoded variants of the AsPC-1 and Panc-89 human cell lines, which were originally derived from patients with metastatic PDAC[30], to assess the impact of these compounds on both cell lines in parallel in the same mouse (**Supplementary Fig. 5a–c**). We screened our top five candidates and identified two compounds (JCP-170 and JCP-265) that robustly and reproducibly inhibited metastatic seeding of the murine cell line 0688M and both human PDAC cell lines (**Fig. 2b–g**, **Supplementary Fig. 5d**,**e**, and **Supplementary Tables 1–3**).

These compounds are substituted chloroisocoumarins, which exhibit very low toxicity in 0688M, AsPC-1, and Panc-89 cells (**Supplementary Figs. 4e** and **6a–c**, **g–i**).

The liver is another major site of metastasis in pancreatic cancer patients[24]. To investigate the importance of our findings to metastatic seeding in additional organs *in vivo*, we quantified the dose-dependent effects of our top candidates on metastatic seeding to the liver after intrasplenic transplantation. Both JCP-265 and JCP-170 inhibited metastatic seeding to the liver after intrasplenic transplantation (**Fig. 2h–j**). The dose-dependent inhibition of liver metastatic seeding was consistent with the intravenous model, mirroring the reduction in metastasis observed in the lung (**Supplementary Fig. 4f**,**g** and **Supplementary Table 4**). These data suggest a general inhibition of metastatic seeding by these compounds and demonstrate the utility of our multiplexed strategy in multiple *in vivo* metastasis models.

Identification of the lipase ABHD6 as a target of JCP-265
To identify the target(s) of our top lead compounds, we employed functional proteomics using activity-based protein profiling–multidimensional protein identification technology (ABPP–MudPIT)[31]. We synthesized several JCP-170 and JCP-265 analogs containing an alkyne functionality compatible with click chemistry (**Supplementary Fig. 7a**,**e**). We used our multiplexed screening platform to determine which analogs maintained antimetastatic activity on murine and human PDAC cell lines *in vivo*. The JCP-265 analog CJS-023 maintained metastatic selectivity
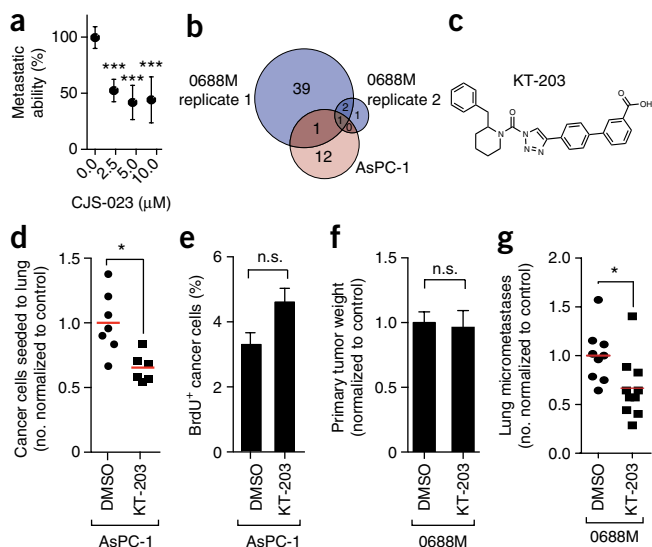
Figure 3 | Identification and validation of ABHD6 as a target of JCP-265. (**a**) Metastatic ability of 0688M cells treated with CJS-023. *n* = 3 per concentration; *n* = 36 for control (0 μM); ***P < 0.001. (**b**) Venn diagram of CJS-023-bound proteins identified by mass spectrometry with ratio scores > 5. (**c**) Structure of KT-203. (**d**) Effect of KT-203 treatment on AsPC-1 cancer cells seeded to the lung, measured by flow cytometry. Normalized data from two independent experiments; *n* = 7 for control, *n* = 6 for treated. Each dot represents one mouse, and the line indicates the mean. *P < 0.05. (**e**) Effect of KT-203 on *in vivo* proliferation of injected cancer cells, measured by flow cytometry. n.s., not significant; *n* = 7 for control; *n* = 6 for treated. (**f,g**) Primary tumor growth (**f**), and number of lung metastases (**g**) in mice with established subcutaneous tumors treated with KT-203 or vehicle. Normalized data from two independent experiments. Each dot represents one mouse and the line indicates the mean. n.s., not significant; *P < 0.05; *n* = 9 for control; *n* = 10 for treated. P values were calculated with the Mann–Whitney test; bar graphs and dots represent the mean ± s.d. For dots that show no error bar, the error bar was smaller than the dot.

and low toxicity *in vitro* across all three cell lines and was selected for target identification (**Fig. 3a**; **Supplementary Figs. 6d**–**f,j**–**l** and **7b**–**d,f**–**h**; and **Supplementary Tables 2** and **3**).

To enable ABPP–MudPIT-based target identification, murine 0688M and human AsPC-1 cells were treated with CJS-023, and probe-bound proteins were enriched by the addition of azido-biotin using click chemistry and subsequent avidin affinity purification. After trypsinization, peptides from CJS-023- and vehicle (DMSO)-treated samples were subjected to stable isotope reductive dimethylation using either heavy or light formaldehyde and pooled prior to combining the samples for MudPIT analysis[32] (**Supplementary Fig. 8a**–**c**). Of the proteins that were enriched in the probe- versus vehicle-treated samples, the serine hydrolase alpha–beta hydrolase domain 6 (ABHD6) was shared between the murine and human data sets and had high sequence coverage (**Fig. 3b**, **Supplementary Fig. 8d,e**, and **Supplementary Table 5**). ABHD6 is a lipase that is best studied in endocannabinoid signaling in the central nervous system[33,34], with other potential roles in metabolic syndrome[35], inflammation[36], and insulin secretion[37]. The importance of ABHD6 in cancer progression or metastasis has yet to be described.

To investigate whether JCP-265 directly binds ABHD6, we performed gel-based competition assays by treating murine

and human PDAC cells with JCP-265, followed by labeling of whole-cell lysates with the fluorescent probe HT01, which labels ABHD6 (ref. 38). We observed dose-dependent competition for HT01 binding to a protein at the expected molecular weight for ABHD6 at single-digit micromolar concentrations (**Supplementary Fig. 9a,b**). JCP-265 also competed with the pan-serine hydrolase reactive chemical probe fluorophosphonate–rhodamine (FP–Rho) for labeling of a protein at the same molecular weight as Abhd6 (**Supplementary Fig. 9e,f**). JCP-170 also competed for ABHD6 probe labeling (**Supplementary Fig. 9b**). To assess whether the chloroisocoumarin scaffold was a non-specific inhibitor of ABHD6, we selected a compound from the library that shared an identical electrophilic functionality with JCP-265 but differed in the western portion of the molecule (JCP-271, **Supplementary Fig. 9c**). This compound was inactive in the initial screening platform, did not show any inhibition of metastatic seeding when tested across a wide dose response, and did not bind the ABHD6 active site (**Supplementary Fig. 9b,d**). *ABHD6* is variably expressed in mouse and human pancreatic cancer tumors and cell lines (**Supplementary Fig. 10**). We confirmed ABHD6 activity in several additional human PDAC cell lines (**Supplementary Fig. 10g**). In conjunction with the proteomics data, this suggests that ABHD6 inhibition contributes to the antimetastatic effect of JCP-265.

ABHD6 inhibition reduces metastatic seeding *in vivo*

To validate ABHD6 as a phenotypically relevant target in *in vivo* models and to avoid potential pleiotropic effects of JCP-265 at higher concentrations, we used a highly selective and potent irreversible ABHD6 inhibitor, KT-203 (ref. 33; **Fig. 3c**), which was not included in the original screening library. Notably, KT-203 also competed for HT01 and FP–Rho binding to the same protein as JCP-265 but was nearly 1,000× more potent than JCP-265 (**Supplementary Fig. 9a,b,e,f**). While JCP-265 was a valuable chemical tool to identify ABHD6 as a driver of metastatic seeding, we focused on KT-203 based on its potency and selectivity for ABHD6 and absence of toxicity when administered to mice[33]. KT-203 competed for ABHD6 labeling at ~1 nM but not for other FP–Rho reactive serine hydrolases even at 100-fold higher concentration (**Supplementary Fig. 9a,b,e,f**). KT-203 treatment of human and mouse PDAC cell lines had no effect on cell growth, proliferation, or apoptosis (**Supplementary Fig. 11**). Since KT-203 covalently inhibits ABHD6, we pre-treated human AsPC-1 pancreatic cancer cells *in vitro* and transplanted them intravenously to assess metastatic seeding. KT-203 pretreatment significantly reduced the number of cancer cells in the lung (*P* < 0.014; **Fig. 3d,e**). Both KT-203- and vehicle-treated cells had minimal and equal proliferation within the metastatic site, suggesting that reduced expansion in the secondary site is not the mechanism by which ABHD6 inhibition reduces cancer cell number. Importantly, KT-203 phenocopies the inhibitory effects observed with JCP-265 despite the structural differences between the two inhibitors, further indicating that ABHD6 is a relevant target.

Subcutaneous growth of 0688M cells leads to robust metastasis to the lung; therefore, we set out to determine whether KT-203 could reduce metastasis from established tumors. We transplanted 0688M cells subcutaneously, allowed tumors to form, and then treated mice with KT-203 (1 mg/kg/d) or vehicle (DMSO).
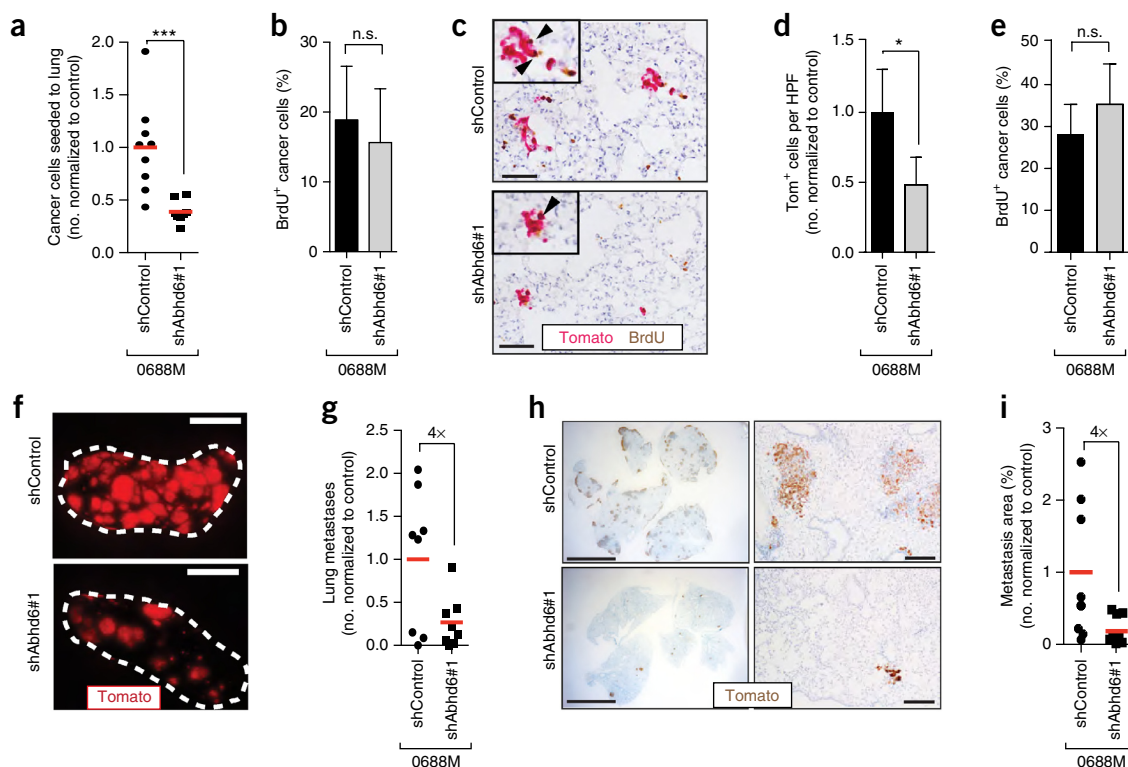
Figure 4 | Knockdown of *Abhd6* decreases metastatic ability of pancreatic cancer cells. (**a**) Metastatic seeding to the lung of 0688M cells with or without *Abhd6* knockdown 48 h after intravenous transplantation, quantified by flow cytometry. Normalized data from two independent experiments; each dot represents one mouse; the line indicates the mean; $n = 9$. ***$P < 0.001$. (**b**) Proliferation of 0688M cells with or without *Abhd6* knockdown seeded in the lung as assessed by flow cytometry. n.s., not significant; $n = 9$. (**c**) Immunohistochemistry for Tomato and BrdU in the lungs of recipient mice (scale bars, 50 μm). BrdU+ cells are indicated with arrowheads. (**d**) Quantification of Tomato+ cancer cells per high power (40×) field (HPF); *$P < 0.05$; Tom, Tomato. (**e**) Quantification of BrdU+ cells. n.s., not significant. (**f**) Representative fluorescent image of one lung lobe of mice transplanted with *Abhd6* knockdown or controls 3 weeks after intravenous transplantation (scale bars, 4 mm). (**g**) Quantification of number of metastases, $P = 0.0545$. Normalized data from two independent experiments is shown. Each dot represents one mouse, and the line indicates the mean; $n = 8$. (**h**) Immunohistochemistry for Tomato in the lungs of recipient mice 3 weeks after injection (scale bars: left panels, 5 mm; right panels, 50 μm). (**i**) Quantification of Tomato+ metastasis. Normalized data from two independent experiments; Each dot represents one mouse and the line indicates the mean, $n = 9$, $P = 0.0379$ P values were calculated using the Mann–Whitney test; All bar graphs represent the mean ± s.d.

Labeling of organ lysates with HT01 confirmed Abhd6 inhibition *in vivo* (**Supplementary Fig. 9g**). Neither the primary tumor growth rate nor histological patterns were affected by KT-203 treatment (**Fig. 3f** and data not shown). However, the number of lung metastases was significantly reduced by KT-203 treatment ($P < 0.012$; **Fig. 3g**). We further investigated cancer cell adhesion and found that KT-203 pretreatment modestly, but reproducibly, reduces adhesion of both mouse and human PDAC cells to endothelial cells *in vitro* (**Supplementary Fig. 12a,b**).

Abhd6 knockdown reduces metastatic seeding *in vivo*

To genetically validate the importance of Abhd6 for optimal metastatic fitness of PDAC cells, we used two independent shRNAs to knockdown *Abhd6* (**Supplementary Fig. 13a–d**). Consistent with results obtained using KT-203, *Abdh6* knockdown had no effect on cell growth, proliferation, or apoptosis (**Supplementary Fig. 13e–g**) but reduced adhesion of PDAC cells to endothelial cells *in vitro* (**Supplementary Fig. 12c**). Importantly, *Abhd6* knockdown reduced lung seeding after intravenous transplantation by ~60% ($P < 0.0003$, **Fig. 4a,c,d** and **Supplementary Fig. 13h,i**). *Abhd6* knockdown did not affect proliferation of the cancer cells at the secondary site (**Fig. 4b,c,e** and **Supplementary Fig. 13i,j**).

To determine whether the reduced metastatic seeding by sh*Abhd6* cells would translate to fewer macrometastases at a later time point, we transplanted ten-fold fewer cells and analyzed the mice after 3 weeks. Overall, 0688Msh*Abhd6*-injected mice had approximately four-fold fewer metastases than 0688Msh*Control*-injected mice (**Fig. 4f–i**). Consistently, *ABHD6* knockdown in AsPC-1 cells with an additional independent shRNA had no effect on cell growth *in vitro*, but metastatic burden was significantly lower in AsPC-1sh*ABHD6*-injected mice (**Supplementary Fig. 14**).

DISCUSSION

Our *in vivo* screening platform is a dramatic improvement over assessing individual compounds in mice *in vivo*. A one-compound-per-mouse strategy quickly becomes resource limiting, which has precluded previous *in vivo* screening of large chemical libraries. Using our platform, we efficiently screened >700 compounds in triplicate, including internal controls, using only 36 mice. In addition to being time, cost and resource efficient, this approach is highly quantitative and greatly reduces the technical variation often encountered with *in vivo* assays. The low variability allowed us to observe subtle differences (20–30%) between compound effects. At the secondary screening stage, multiple

compounds were screened across six doses in a single mouse, which allowed direct comparisons of compound potency. Many of these assays were conducted months apart and were highly reproducible. The exogenous pretreatment of cells before introduction *in vivo* also negated any systemic effects of compound treatment of the mice themselves, thus ensuring that the observed phenotype was cell autonomous.

Our platform can easily be adapted to screen compounds (or any other pretreatment) in a combinatorial matrix, which could identify synergistic, additive, or antagonistic combinations. Based on the parameters of our screen (~2,000 cells with each barcode recovered from each mouse and 11% s.d. between mice), increasing the number of barcoded cell lines to 384 would only increase the mouse-to-mouse variability to ~16%. Therefore, a further increase in throughput is feasible.

Our results validate the generalizability of this approach. We screened three different cell lines, including two differentially barcoded human cell lines in the same recipient mice. We used different routes of injection, demonstrating that different sites of metastatic seeding can be interrogated. Given the facile nature of screening using this platform, libraries could also be screened across isogenic cell lines of different genotypes to uncover context-specific effects, which could provide insight into the involvement of unknown pathways based on their differential activities in the screen.

While this platform can be used to identify novel drug leads, it also allows the investigation of underlying mechanisms of a complex biological process. Our proof-of-principle application identified the lipase ABHD6 as a regulator of metastatic seeding of PDAC. In the nervous system, ABHD6 modulates endocannabinoid signaling; however, ABHD6 is expressed in many cell types where it has different lipid substrates[37,39,40]. A similar enzyme, MAGL, contributes to a pathogenic lipid signature in cancer[41,42], and high ABHD6 expression correlates with increased metastatic ability in some cancer types[43]. Our data suggest that dysregulation of lipid networks could represent an important aspect of metastatic colonization. While ideal antimetastatic drugs would likely inhibit both colonization and growth of existing metastases, a further mechanistic understanding of the metastatic process is paramount for the development of antimetastatic therapies[44].

Beyond the application to cancer and small-molecule screening, our platform can be applied in any situation where cells can be barcoded and an *in vitro* perturbation results in sustained effects after pooling. In our initial application, the covalent nature of the compounds in our library led to sustained target inhibition. Even reversible inhibitors that perturb cellular homeostasis (e.g., gene expression, signaling pathway changes, or accumulation of enzyme substrates) could theoretically be screened using this platform (**Supplementary Fig. 15**). This platform could also be applied to screen-directed changes in gene expression or perturbation of protein function, such as siRNA or cDNA transfections. We envision other applications in diverse fields including immunology, stem cell research, and in the investigation of infectious diseases. This strategy should open the door to screens to identify drivers or inhibitors of many *in vivo* processes across diverse fields of study.

METHODS

Methods and any associated references are available in the online version of the paper.

Note: Any Supplementary Information and Source Data files are available in the online version of the paper.

AUTHOR CONTRIBUTIONS

B.M.G., C.J.S., M.B., and M.M.W. conceived the study and designed the experiments. B.M.G., C.J.S., D.Y., M.M.D. C.-H.C. and S.-H.C. performed experiments; C.D.M. and Z.N.R. conducted bioinformatics; D.O. synthesized KT-203; and B.M.G. and C.J.S. analyzed the data. J.M.B. contributed reagents. B.F.C. provided reagents and critical insight. M.B. and M.M.W. oversaw the project. B.M.G., C.J.S., M.B., and M.M.W. wrote the manuscript with comments from all authors.

COMPETING FINANCIAL INTERESTS

The authors declare no competing financial interests.

Reprints and permissions information is available online at http://www.nature.com/reprints/index.html.

1. Schirle, M. & Jenkins, J.L. Identifying compound efficacy targets in phenotypic drug discovery. *Drug Discov. Today* **21**, 82–89 (2016).
2. Bassilana, F. *et al.* Target identification for a Hedgehog pathway inhibitor reveals the receptor GPR39. *Nat. Chem. Biol.* **10**, 343–349 (2014).
3. Chen, X., Barclay, J.W., Burgoyne, R.D. & Morgan, A. Using *C. elegans* to discover therapeutic compounds for ageing-associated neurodegenerative diseases. *Chem. Cent. J.* **9**, 65 (2015).
4. Rennekamp, A.J. & Peterson, R.T. 15 years of zebrafish chemical screening. *Curr. Opin. Chem. Biol.* **24**, 58–70 (2015).
5. Hannan, S.B., Dräger, N.M., Rasse, T.M., Voigt, A. & Jahn, T.R. Cellular and molecular modifier pathways in tauopathies: the big picture from screening invertebrate models. *J. Neurochem.* **137**, 12–25 (2016).
6. Jonas, O. *et al.* An implantable microdevice to perform high-throughput *in vivo* drug sensitivity testing in tumors. *Sci. Transl. Med.* **7**, 284ra57 (2015).
7. Klinghoffer, R.A. *et al.* A technology platform to assess multiple cancer agents simultaneously within a patient's tumor. *Sci. Transl. Med.* **7**, 284ra58 (2015).
8. Wagenblast, E. *et al.* A model of breast cancer heterogeneity reveals vascular mimicry as a driver of metastasis. *Nature* **520**, 358–362 (2015).
9. Bhang, H.E. *et al.* Studying clonal dynamics in response to cancer therapy using high-complexity barcoding. *Nat. Med.* **21**, 440–448 (2015).
10. Lu, R., Neff, N.F., Quake, S.R. & Weissman, I.L. Tracking single hematopoietic stem cells *in vivo* using high-throughput sequencing in conjunction with viral genetic barcoding. *Nat. Biotechnol.* **29**, 928–933 (2011).
11. Naik, S.H. *et al.* Diverse and heritable lineage imprinting of early haematopoietic progenitors. *Nature* **496**, 229–232 (2013).
12. Fan, H.C., Fu, G.K. & Fodor, S.P. Expression profiling. Combinatorial labeling of single cells for gene expression cytometry. *Science* **347**, 1258367 (2015).
13. Yu, C. *et al.* High-throughput identification of genotype-specific cancer vulnerabilities in mixtures of barcoded tumor cell lines. *Nat. Biotechnol.* **34**, 419–423 (2016).

14. Siegel, R.L., Miller, K.D. & Jemal, A. Cancer statistics, 2015. *CA Cancer J. Clin.* **65**, 5–29 (2015).
15. Jones, S. *et al.* Core signaling pathways in human pancreatic cancers revealed by global genomic analyses. *Science* **321**, 1801–1806 (2008).
16. Moffitt, R.A. *et al.* Virtual microdissection identifies distinct tumor- and stroma-specific subtypes of pancreatic ductal adenocarcinoma. *Nat. Genet.* **47**, 1168–1178 (2015).
17. Knudsen, E.S., O'Reilly, E.M., Brody, J.R. & Witkiewicz, A.K. Genetic diversity of pancreatic ductal adenocarcinoma and opportunities for precision medicine. *Gastroenterology* **150**, 48–63 (2015).
18. Yachida, S. & Iacobuzio-Donahue, C.A. The pathology and genetics of metastatic pancreatic cancer. *Arch. Pathol. Lab. Med.* **133**, 413–422 (2009).
19. Yachida, S. *et al.* Distant metastasis occurs late during the genetic evolution of pancreatic cancer. *Nature* **467**, 1114–1117 (2010).
20. Whittle, M.C. *et al. RUNX3* controls a metastatic switch in pancreatic ductal adenocarcinoma. *Cell* **161**, 1345–1360 (2015).
21. Guan, X. Cancer metastases: challenges and opportunities. *Acta Pharm. Sin. B* **5**, 402–418 (2015).
22. Zhang, Y., Zhang, W. & Qin, L. Mesenchymal-mode migration assay and antimetastatic drug screening with high-throughput microfluidic channel networks. *Angew. Chem. Int. Ed. Engl.* **53**, 2344–2348 (2014).
23. Colas, P. High-throughput screening assays to discover small-molecule inhibitors of protein interactions. *Curr. Drug Discov. Technol.* **5**, 190–199 (2008).
24. Budczies, J. *et al.* The landscape of metastatic progression patterns across major human cancers. *Oncotarget* **6**, 570–583 (2015).
25. Hingorani, S.R. *et al. Trp53^{R172H}* and *Kras^{G12D}* cooperate to promote chromosomal instability and widely metastatic pancreatic ductal adenocarcinoma in mice. *Cancer Cell* **7**, 469–483 (2005).
26. Hingorani, S.R. *et al.* Preinvasive and invasive ductal pancreatic cancer and its early detection in the mouse. *Cancer Cell* **4**, 437–450 (2003).
27. Arastu-Kapur, S. *et al.* Identification of proteases that regulate erythrocyte rupture by the malaria parasite Plasmodium falciparum. *Nat. Chem. Biol.* **4**, 203–213 (2008).
28. Hall, C.I. *et al.* Chemical genetic screen identifies Toxoplasma DJ-1 as a regulator of parasite secretion, attachment, and invasion. *Proc. Natl. Acad. Sci. USA* **108**, 10568–10573 (2011).
29. Child, M.A. *et al.* Small-molecule inhibition of a depalmitoylase enhances *Toxoplasma* host-cell invasion. *Nat. Chem. Biol.* **9**, 651–656 (2013).
30. Sipos, B. *et al.* A comprehensive characterization of pancreatic ductal carcinoma cell lines: towards the establishment of an *in vitro* research platform. *Virchows Arch.* **442**, 444–452 (2003).
31. Jessani, N. *et al.* A streamlined platform for high-content functional proteomics of primary human specimens. *Nat. Methods* **2**, 691–697 (2005).
32. Boersema, P.J., Raijmakers, R., Lemeer, S., Mohammed, S. & Heck, A.J. Multiplex peptide stable isotope dimethyl labeling for quantitative proteomics. *Nat. Protoc.* **4**, 484–494 (2009).
33. Hsu, K.L. *et al.* Discovery and optimization of piperidyl-1,2,3-triazole ureas as potent, selective, and *in vivo*-active inhibitors of α/β-hydrolase domain containing 6 (ABHD6). *J. Med. Chem.* **56**, 8270–8279 (2013).
34. Marrs, W.R. *et al.* The serine hydrolase ABHD6 controls the accumulation and efficacy of 2-AG at cannabinoid receptors. *Nat. Neurosci.* **13**, 951–957 (2010).
35. Thomas, G. *et al.* The serine hydrolase ABHD6 is a critical regulator of the metabolic syndrome. *Cell Rep.* **5**, 508–520 (2013).
36. Alhouayek, M., Masquelier, J., Cani, P.D., Lambert, D.M. & Muccioli, G.G. Implication of the anti-inflammatory bioactive lipid prostaglandin D2-glycerol ester in the control of macrophage activation and inflammation by ABHD6. *Proc. Natl. Acad. Sci. USA* **110**, 17558–17563 (2013).
37. Zhao, S. *et al.* α/β-hydrolase domain-6-accessible monoacylglycerol controls glucose-stimulated insulin secretion. *Cell Metab.* **19**, 993–1007 (2014).
38. Hsu, K.L. *et al.* DAGLβ inhibition perturbs a lipid network involved in macrophage inflammatory responses. *Nat. Chem. Biol.* **8**, 999–1007 (2012).
39. Thomas, G., Brown, A.L. & Brown, J.M. *In vivo* metabolite profiling as a means to identify uncharacterized lipase function: recent success stories within the alpha beta hydrolase domain (ABHD) enzyme family. *Biochim. Biophys. Acta* **1841**, 1097–1101 (2014).
40. Pribasnig, M.A. *et al.* α/β hydrolase domain-containing 6 (ABHD6) degrades the late endosomal/lysosomal lipid bis(monoacylglycero)phosphate. *J. Biol. Chem.* **290**, 29869–29881 (2015).
41. Nomura, D.K. *et al.* Monoacylglycerol lipase exerts dual control over endocannabinoid and fatty acid pathways to support prostate cancer. *Chem. Biol.* **18**, 846–856 (2011).
42. Nomura, D.K. *et al.* Monoacylglycerol lipase regulates a fatty acid network that promotes cancer pathogenesis. *Cell* **140**, 49–61 (2010).
43. Max, D., Hesse, M., Volkmer, I. & Staege, M.S. High expression of the evolutionarily conserved alpha/beta hydrolase domain containing 6 (ABHD6) in Ewing tumors. *Cancer Sci.* **100**, 2383–2389 (2009).
44. Steeg, P.S. Targeting metastasis. *Nat. Rev. Cancer* **16**, 201–218 (2016).

ONLINE METHODS

Generation and selection of murine PDAC cell lines for multiplexed screening. We generated polyclonal cell lines from primary tumors and metastases that formed in the autochthonous $Kras^{LSL-G12D/+}$;$Trp53^{LSL-R172H/+}$;$Rosa26^{LSL-tdTomato/+}$;$Pdx1-Cre$ pancreatic cancer mouse model[25,26]. To establish the cell lines, a piece of the primary tumor or the macrometastasis was dissected, washed twice with cold PBS, minced with a scalpel, and transferred to a tissue culture dish containing DMEM media (high glucose with 10% fetal bovine serum (FBS) and antibiotics). Cells were allowed to attach, and they were grown for 1 week with two media changes. Then cells were passaged at least three times to select away from fibroblast contamination. Purity was confirmed by FACS (tdTomato), and MycoAlert Mycoplasma detection kit (Lonza) was used to verify the lack of mycoplasma contamination. To select which cell line to use for the multiplexed screening platform, 10^6 cells from each of the following cell lines: 0688M (liver metastasis), 0748PF (ascites fluid), and 0755P (primary pancreatic tumor) were injected into the lateral tail vein of one male 129/Bl6 F1 mouse per cell line (Jackson Laboratories, Stock number 101043). Lungs were harvested after 24 h, and the number of cells that seeded the lungs was assessed by fluorescence microscopy. 0755P showed very low seeding ability and was therefore excluded. To further test metastatic ability, 5×10^5 0748PF or 0688M cells were injected into the lateral tail vein of one male 129/Bl6 F1 mouse per cell line and allowed to grow for 2.5 weeks. Lungs were harvested and assessed for metastatic burden. 0688M cells showed a higher metastatic ability. The 0688M cell line was further tested by injecting 5×10^4 cells into the lateral tail vein of three male 129/Bl6 F1 mice. Lungs were harvested, and the number of metastases in the lungs was counted after 4 weeks (~200 per mouse). The robust phenotype of this cell line confirmed its applicability for the *in vivo* screening platform.

Generation of barcoded pancreatic cancer cell line variants. To generate barcoded variants of retroviral vector (MSCV–GFP/Puro) we PCR amplified a region of the vector with primers designed to add a random six-nucleotide barcode. Ligation of this fragment into the parent vectors generated approximately 180 unique retroviral MSCV–BC–GFP/Puro vectors (**Supplementary Fig. 1**). Individual plasmid preparations (Qiagen Miniprep kit) were analyzed by Sanger sequencing of the barcode region. 120 uniquely barcoded plasmids were used to generate barcoded cell lines. MSCV retroviral vectors were generated using pCL-Eco for infection of the murine pancreatic cancer cell line 0688M. For virus production, HEK293T cells were seeded into six-well plates, and individual wells were transfected at 80% confluency with MSCV–BC–GFP/Puro vector and packaging plasmids using TransIT-TKO Transfection Reagent (Mirus). Media was changed 24 h later. Supernatants were collected at 48 and 72 h, pooled, centrifuged for 10 min at 13,200 r.p.m., and the undiluted supernatants were each applied to a 70% confluent well 0688M cells in six-well plates. 2 d after infection the cells were selected with puromycin (8 µg/mL), which effectively kills all uninfected cells. Infection rates were >70% for each cell line variant before puromycin selection (and >99% after selection), indicating that a diverse population of cells gave rise to each barcoded cell line.

After puromycin selection, cell lines were expanded and tested for GFP expression using FACS. 96 cell lines were chosen for the final barcode layout based on GFP expression (>98%) and similar growth rates. Cells were mixed with freezing media (FBS containing 10% DMSO) and frozen unattached in 96-well plates in three different plate layouts in multiple copies (**Supplementary Fig. 2**). Cell line plates were thawed for 10 min at 37 °C, centrifuged to remove freezing media and recovered overnight in fresh media. Cells were split 1:2 onto fresh plates after 24 h and split again 1:3 48 h later for overnight recovery before compound treatment.

Compound treatment, pooling, and transplantation. Compounds were diluted in DMSO in 96-well master plates to 1 mM stock concentrations. Each plate contained ~60–70 compounds and ~26–36 DMSO-containing control wells (**Supplementary Fig. 2**). 2 µl of each compound was added to the barcoded cells using an Agilent (formerly Velocity11) vertical pipetting station with a 96LT pipetting head to a final concentration of 10 µM. Each compound plate was tested in triplicate using three different cell plate layouts to exclude specific barcode–compound pairing biases (**Supplementary Fig. 2**). Cells were treated for 6 h at 37 °C, media was removed, cells were washed once with PBS, and cells were trypsinized for 5 min. All cells of one plate were pooled, centrifuged, counted, and diluted to approximately 5×10^6 cells per ml in PBS. 200 µl of cells (~10^6) from each plate were injected into the lateral tail vein of one male 129/Bl6 F1 mouse (Jackson Laboratories, stock number 101043). The remaining cells (~200 µl) were pelleted and frozen for preinjection barcode representation analysis. For intrasplenic transplant, 10^6 cells were resuspended in 50 µl PBS and injected into male 129/Bl6 F1 mice using standard methods[45].

Cancer cell isolation. 48 h after intravenous or intrasplenic transplantation of the compound-treated, pooled pancreatic cancer cells, lungs (intravenous) or livers (intrasplenic) were harvested. Each lung or liver was minced using scissors and digested for 1 h at 37 °C in digestion media with 10% trypsin (0.25% in EDTA, Invitrogen), 10% collagenase IV (10 mg/ml in HBSS, Worthington) and 10% dispase (Corning) in HBSS without Ca^{2+} and Mg^{2+}. Digest was quenched with L15 media (Invitrogen) containing 10% FBS and DNase (5 mg/ml in HBSS), and suspension was filtered through a 40 µm mesh, centrifuged, washed, and filtered again. Samples were sorted for Tomato$^+$ (mouse) or GFP$^+$ (human) cells. Cell sorting was performed on FACSAria sorters (BD Biosciences).

Barcode amplification and sequencing for representation. DNA from frozen cell pellets (preinjection and postseeding) was isolated using the Puregene core kit (Qiagen). Using 50% of the isolated DNA, the genetic barcode region was amplified with primers that added the Illumina sequencing primer binding sites and adapters as well as multiplexing tags in a single 30 cycle PCR reaction. PCR products were separated on agarose gels and gel purified using the Qiagen gel extraction kit. PCR products were eluted twice in 30 µl ddH$_2$O, and concentration was measured using the Qubit dsDNA HS assay kit (Invitrogen). For each MiSeq run, 12 samples were pooled in equal concentrations, mixed with 50% PhiXv3 control, and single reads were sequenced using the MiSeqV3-150 bp kit on a Illumina MiSeq sequencer. Reads per barcode per sample were extracted from the fastq files and preinjection to postseeding barcode ratios were calculated. Each tested compound plate was

normalized to the average of all DMSO controls included on that plate. Since all compounds were tested in triplicate, the average metastatic ability per compound was calculated in comparison to DMSO-treated controls. Calculations were automated using purpose-built python code.

When running a DMSO-only plate to assess overall untreated s.d. it was observed that three barcodes (25, 84, and 97) were always over-represented in the postseeding sample, independent from their position on the plate. Therefore, these three barcodes were excluded from further analysis, leading to only duplicate values for three compounds and six DMSO controls on each test plate.

Primers: 5′→3′

BG#12, universal forward AATGATACGGCGACCACCGAG ATCTACACTCTTTCCCTACACGACGCTCTTCCGATCTTCT AGGCGCCGGAATTAGATCC

BG#13MP1, indexed reverse CAAGCAGAAGACGGCATACG AGATCGTGATGTGACTGGAGTTCAGACGTGTGCTCTTCC GATCAGCTCGACCAGGATGGGCAC

BG#13MP2, indexed reverse CAAGCAGAAGACGGCATACG AGATACATCGGTGACTGGAGTTCAGACGTGTGCTCTTCC GATCAGCTCGACCAGGATGGGCAC

BG#13MP3, indexed reverse CAAGCAGAAGACGGCATACG AGATGCCTAAGTGACTGGAGTTCAGACGTGTGCTCTTCC GATCAGCTCGACCAGGATGGGCAC

BG#13MP4, indexed reverse CAAGCAGAAGACGGCATACG AGATTGGTCAGTGACTGGAGTTCAGACGTGTGCTCTTCC GATCAGCTCGACCAGGATGGGCAC

BG#13MP5, indexed reverse CAAGCAGAAGACGGCATACG AGATTACTGTGTGACTGGAGTTCAGACGTGTGCTCTTCC GATCAGCTCGACCAGGATGGGCAC

BG#13MP6, indexed reverse CAAGCAGAAGACGGCATACG AGATATTGGCGTGACTGGAGTTCAGACGTGTGCTCTTCC GATCAGCTCGACCAGGATGGGCAC

BG#13MP7, indexed reverse CAAGCAGAAGACGGCATACG AGATGATCTGGTGACTGGAGTTCAGACGTGTGCTCTTCC GATCAGCTCGACCAGGATGGGCAC

BG#13MP8, indexed reverse CAAGCAGAAGACGGCATACG AGATTCAAGTGTGACTGGAGTTCAGACGTGTGCTCTTCC GATCAGCTCGACCAGGATGGGCAC

BG#13MP9, indexed reverse CAAGCAGAAGACGGCATACG AGATCTGATCGTGACTGGAGTTCAGACGTGTGCTCTTCC GATCAGCTCGACCAGGATGGGCAC

BG#13MP10, indexed reverse CAAGCAGAAGACGGCATAC GAGATAAGCTAGTGACTGGAGTTCAGACGTGTGCTCTTC CGATCAGCTCGACCAGGATGGGCAC

BG#13MP11, indexed reverse CAAGCAGAAGACGGCATAC GAGATGTAGCCGTGACTGGAGTTCAGACGTGTGCTCTTC CGATCAGCTCGACCAGGATGGGCAC

BG#13MP12, indexed reverse CAAGCAGAAGACGGCATAC GAGATTACAAGGTGACTGGAGTTCAGACGTGTGCTCTTC CGATCAGCTCGACCAGGATGGGCAC

Human cell line barcodes and injections. Human pancreatic cancer cell lines AsPC-1 and Panc89 (also referenced as T3M4) have both been described previously[30], and cell line identities were validated by Genetica DNA Laboratories using STR analysis and negative tested for mycoplasma contamination. Each cell line was labeled with 40 unique barcode-GFP-containing retroviral vectors (as used previously for generating the murine cell lines).

MSCV retroviral vectors were generated using gag/pol-retro and VSV-G-retro packaging plasmids. Virus production and infection were performed as described above. After selection for 48 h with puromycin (3 μg/ml), cells were expanded and tested for robust GFP expression using FACS. All cell line variants of both cell lines that passed the quality control (GFP+ > 98%) were distributed onto separate 96-well plates and frozen as described above. For testing of compounds, plates were thawed as described above and split 1:2 after 24 h recovery and again split 1:2 after additional 48 h. Cells were treated with compounds as described above for 6 h. All compounds were tested on variants of both parental cell lines. After treatment, cells were washed with PBS and trypsinized. All cells of both AsPC-1 and Panc89 plates that were treated with the same compound plate were combined, centrifuged, resuspended in PBS, and counted. Cells were diluted to approximately 5×10^6 cells per ml in 400 μl, half were injected into one recipient NOD/Scid/γC (NSG) mouse, and the remaining cells were pelleted and frozen for preinjection barcode representation. DNA extraction and Illumina MiSeq sequencing were performed as described above.

Gel-based competition profiling. Cells were seeded into 12-well plates (100,000 cells per well) in DMEM supplemented with 10% FBS and incubated at 37 °C and 5% CO_2 overnight. Cells were treated *in situ* with either vehicle (DMSO) or compound and incubated at 37 °C for 4 h. After the treatment period, cells were washed with PBS, trypsinized, resuspended in DMEM + 10% FBS, and pelleted at 4 °C. Cell pellets were washed twice with cold PBS and lysed in 20 μl lysis buffer (PBS, 1% NP-40, 0.1% SDS) on ice for 1 h. Lysates were centrifuged at 13,000 r.p.m. for 30 min at 4 °C. Total protein concentration was assessed using the BCA protein assay kit (Pierce). Lysates (25 μg for 0688M cells, 15 μg for AsPC-1 cells) were labeled in 20 μl final reaction volume with either HT-01 or FP-Rhodamine (1 μM final concentration) for 30 min at 37 °C. The reactions were quenched with SDS–PAGE loading buffer and boiled for 5 min. After separation with SDS–PAGE (15% acrylamide), gels were visualized using a flatbed fluorescent scanner (Typhoon, GE Healthcare Life Sciences). Assessment of ABHD6 activity in the shRNA knockdown cell lines (0688M and AsPC-1) was performed using a similar protocol with the exception of compound treatment. Assessment of organ and tumor labeling was performed by lysis of whole organs in PBS using sonication and following the above protocol. Gels were stained with Coomassie to determine equal loading. Relative activity of ABHD6 was assessed by quantification of band intensity using ImageJ. Values were normalized to the average of three replicate vehicle (DMSO)-treated lanes. Each compound concentration is expressed as the average of biological triplicate measurements.

Assessment of *in vitro* cytotoxicity. Cells were seeded into 96-well plates (2,000 cells/well) in 200 μl DMEM supplemented with 10% FBS and incubated at 37 °C and 5% CO_2 overnight. Compounds were added (2 μl, 1% final DMSO concentration), and plates were incubated at 37 °C and 5% CO_2 for 6 h. PR-171 (10 μM) and a well with media only were included as controls. After the incubation period, the compound-containing media was removed, and 100 μl DMEM + 10% FBS was added. After 42 h, cell viability was assessed using the CellTiter-Blue cell viability assay (Promega) per manufacturer's instructions. Cells were incubated

with 10 µl of the CellTiter-Blue reagent for 4 h, and fluorescence was assessed using a Cytation 3 plate reader (Bio-Tek). Data were normalized to the average of vehicle control wells ($n = 12$) in each plate and calculated as percent relative growth.

ABPP sample preparation. AsPC-1 and 0688M cells were grown to ~75% confluence in DMEM supplemented with 10% FBS in 15 cm dishes. Cells were treated *in situ* with either CJS-023 (10 µM) or vehicle (DMSO) for 2 h at 37 °C. After the treatment period, cells were washed three times with PBS. Ice-cold PBS (8 mL) was added, and cells were harvested by scraping. The cells were pelleted by centrifugation at 1,400 g for 3 min at 4 °C. The supernatant was removed, and cell pellets were flash frozen in liquid N_2 for processing. The cell pellet was resuspended in 1 mL ice-cold PBS and lysed by sonication on ice. The protein concentration was determined using a protein assay kit (Bio-Rad) and the proteome was diluted with PBS to 2 mg/mL in 1 mL total volume. To perform the click reaction with biotin azide, 20 µl of a 50 mM $CuSO_4$ solution, 60 µl TBTA (1.7 mM in 1:4 tBuOH:DMSO), 20 µl of 5 mM biotin azide solution in DMSO, and 20 µl of 50 mM TCEP solution were added to each 2 mg of protein. The mixture was vortexed and placed on a rotator at room temperature for 1 h. After the incubation period, 2 mL cold MeOH was added to each sample, followed by 0.5 mL cold $CHCl_3$, and 1 mL cold PBS and vortexed. The samples were centrifuged at 4,200 r.p.m. for 10 min. The liquid was aspirated, and the protein disc was washed 3× with 1:1 MeOH:$CHCl_3$. The pellet was resuspended in 4:1 MeOH:$CHCl_3$ and centrifuged at 4,200 r.p.m. for 10 min, and the supernatant was aspirated. The pellet was denatured in 6 M urea in PBS and 20 µl of 10% SDS, reduced by the addition of premixed TCEP (100 mM) and K_2CO_3 (300 mM) and incubated on a shaker at 37 °C. Finally, the sample was alkylated by the addition of iodoacetamide (55 µM) and incubated for 30 min at room temperature in the dark. For the avidin enrichment, samples were diluted with 5.5 mL of PBS and 200 µl of 5% SDS. Avidin beads (Sigma A-9207) were washed 3× with PBS, and 100 µl of washed beads was added to each sample and incubated at room temperature for 1.5 h with rotation. The beads were washed with 3 × 10 mL of 0.2% SDS in PBS, 3 × 10 mL PBS, and 3 × 10 mL ddH$_2$O. Beads were transferred to protein LoBind eppendorf tubes using TEAB (100 mM in H_2O), centrifuged, and the supernatant was aspirated. The tryptic digestion was performed by the addition of 3 µl of a 0.5 µg/µl trypsin solution and 200 µl of a 2 M urea solution in TEAB to each sample. The samples were incubated overnight on a shaker at 37 °C.

Reductive dimethylation labeling. Either 10 µl 4% CH_2O (light) or 10 µl 4% $^{13}CH_2O$ (heavy), followed by 10 µl of 0.6 M NaBH$_3$CN was added to each pair of vehicle and CJS023-treated replicates. The light/heavy labeling was alternated between each pair of vehicle-treated samples. The tubes were vortexed gently for 2 h at room temperature. Reactions were quenched using 40 µl of 1% ammonium hydroxide. The appropriate light/heavy sample pairs were mixed, centrifuged, and the supernatants were transferred to LoBind eppendorf tubes. 20 µl of formic acid was added to quench and acidify, and samples were spun at 17,000 g for 2 min and transferred to clean tubes for MudPIT analysis. Mass spectrometry was performed using a Thermo Orbitrap mass spectrometer following previously described protocols[46].

Peptides were pressure loaded onto an in-house-made 250 µm desalting salting column which was connected to a 100 µm fused silica capillary column with a 5 µm tip that contained 10 cm of C18 resin (Aqua 5 µm, Phenomenex) and 3 cm of SCX resin (Luna 5 µm, Phenomenex). Peptides were eluted using a five-step multidimensional LC–MS (MudPIT) protocol[47]. The gradients for identification of probe-labeled proteins consisted of increasing salt bumps of 25%, 50%, 80%, and 100% 500 mM ammonium acetate followed by an increasing gradient of acetonitrile and 0.1% formic acid. For all samples, data were collected in data-dependent acquisition mode over a range from 400–1,800 *m/z*. Each full scan was followed by seven fragmentation events. Dynamic exclusion was enabled (repeat count of 1, exclusion duration of 20 s) for all experiments. The data were searched using the ProLuCID algorithm against a human or mouse reverse-concatenated nonredundant (gene-centric) FASTA database that was assembled from the Uniprot database. ProLuCID searches specified static modification of cysteine residues (+57.0215 *m/z*; iodoacetamide alkylation) and required peptides to contain at least one tryptic terminus. Each data set was independently searched with light and heavy parameter files; for the light search, static modifications on lysine (+28.0313 *m/z*) and N termini (+28.0313 *m/z*) were specified; for the heavy search, static modifications on lysine (+34.06312 *m/z*) and N termini (+34.06312 *m/z*) were specified. The resulting matched MS_2 spectra were assembled into protein identifications, then filtered using DTASelect (version 2.0.47). Peptides were restricted to a specified false-positive rate of ≤1%. Peptide ratios were quantified using in-house software as previously described (CIMAGE)[48]. Peptides detected as singletons, where only the heavy or light isotopically labeled peptide was detected and sequenced, were given a standard ratio of 20, which is the maximum ratio reported here.

***In vitro* cellular assays.** To assess proliferation *in vitro*, cells were seeded overnight and labeled with BrdU at 70% confluency (1 mM final concentration for 4 h). Cells were harvested and stained for BrdU using the BD Pharmingen-APC BrdU Flow Kit (BD Biosciences) according to the manufacturer's protocol. Cells were analyzed by FACS using an LSR.II analyzer. Cell death of cells seeded overnight was assessed using the Annexin V Apoptosis Detection Kit (eBioscience) according to the manufacturer's instructions. Cells were analyzed by FACS on a LSR.II analyzer. Cell growth was measured using the Presto Blue assay from Invitrogen according to the manufacturer's instructions. Cells were treated with compounds at the indicated concentrations.

Adhesion assays were performed using immortalized Human Umbilical Vein Endothelial Cells (HUVEC, hTert transformed) grown to 100% confluency in 24-well plates (with EGM-2 BulletKit media, Lonza). AsPC-1 cells were labeled with CellTracker Green dye (Molecular Probes) at a final concentration of 5 µm for 30 min at 37 °C in serum-free DMEM and washed twice with PBS; for 0688M cells the inherent tdTomato was used as fluorescent marker. 10^4 cancer cells in 50 µl media per well HUVEC were added for 20 min while plates were kept on a plate shaker. Wells were washed twice with PBS, and fluorescent images were taken (10× objective, LEICA DMI 6000B). Data were analyzed counting cell number per optical field using ImageJ. Cancer cells (where indicated) were pretreated overnight with 40 nM KT-203 or DMSO control.

Cell numbers are reported as the average of replicates. All cell culture assays were performed in triplicate or quadruplicate in three independent experiments. Cells were always treated with vehicle (DMSO) or the indicated compounds for the indicated time duration.

ABHD6 expression data analysis. RNA-Seq was performed for primary tumors and metastases that develop in $Kras^{LSL-G12D/+}$; $p53^{LSL-R172H/+}$;$Rosa26^{LSL-tdTomato/+}$;$Pdx1$-Cre mice. Cell sorting was performed on FACSAria sorters (BD Biosciences). Tomato$^+$, lineage$^-$ (CD31, CD45, Ter-119, F4/80), viable (DAPI$^-$) cancer cells as well as the Tomato$^+$ lineage$^-$ viable stromal cells (S.-H.C. and M.M.W., unpublished data set) were compared.

$ABHD6$ expression was interrogated in the data sets published by Moffitt *et al.*[16] as well as the data sets from Cancer Cell Line Encyclopedia (CCLE)[49], TCGA (http://cancergenome.nih.gov/ and extracted from http://www.cbioportal.org) and ICGC (https://dcc.icgc.org). For both microarray and the RNA-Seq data, the data sets were queried for $ABHD6$ expression, and the expression values per case per group were plotted.

Lentiviral knockdown, qRT-PCR and western blotting. $ABHD6$/$Abhd6$ was knocked down using pLKO lentiviral vectors; mouse sh$Abhd6$#1 (TRCN0000375660), mouse sh$Abhd6$#2 (TRCN0000032794), and human sh$ABHD6$ (TRCN0000154639). The control vector was pLKO-shEmpty. Lentivirus was generated using Delta8.2 and VSV-G packaging plasmids. Virus particles were generated and infection, and selection of 0688M and AsPC-1 cells was performed as described above. $Abhd6$ knockdown was confirmed by qPCR and western blotting. qRT-PCR for mouse $Abhd6$ and $Gapdh$ were performed using Taqman probes (Mm00481199_m1 and Mm99999915_g1, respectively, from Applied Biosystems) using standard methods. Human $ABHD6$ ($hABHD6$Fwd CACAAACCCTCCATCCTCAT, $hABHD6$Rev ACCAAGTGCAGGTTCTTTGG) gene expression levels were assessed using standard SYBR green qPCR protocols and normalized to human $ACTIN$ ($hACTIN$Fwd CCTTGCACATGCCGGAG, $hACTIN$Rev GCACAGAGCCTCGCCTT).

For western blotting, denatured protein samples were run on a 4–12% Bis-Tris gel (NuPage) and transferred onto PVDF membrane. Membranes were immunoblotted using primary antibodies against Hsp90 (1:10,000 dilution, BD Transduction Laboratories, 610419) and Abhd6 (1:1,000 dilution, characterized in ref. 33). Primary antibody incubations were followed by secondary HRP-conjugated anti-mouse (1:10,000 dilution, Santa Cruz Biotechnology, sc-2005) and anti-rabbit (1:10,000 dilution, Santa Cruz Biotechnology, sc-2004) antibodies, and membranes were developed with ECL 2 Western Blotting Substrate (P180196, ThermoScientific Pierce).

Transplantation assays and quantification. For intravenous transplantation 10^6 (for 5 min or 2 d) or 5 ×10^4 (for 3 weeks) 0688M or AsPC-1 cells (pretreated 24 h with 40 nM KT-203 or DMSO) in 200 µl PBS were injected into the lateral tail vein of male 129/Bl6 F1 mice (Jackson Laboratories, Stock number 101043) for murine 0688M cells or NOD/Scid/γC (NSG) mice for human AsPC-1 cells. Four to five mice were used per individual experiment per group. No randomization was used as all mice were exactly the same age and genetic background. No blinding or

exclusion criteria were applied. For subcutaneous injections 10^5 0688M cells in 100 µl PBS/matrigel 1:1 were injected into each flank and shoulder of NOD/Scid/γC (NSG) mice. Intravenously injected mice were analyzed 2 or 21 d after transplantation as indicated. For 2 d analyses, lungs were digested and cells isolated as described above and analyzed using a LSR II analyzer (BD) for Tomato$^+$ cells (0688M) or stained with an antibody to human HLA-A,B,C (W6/32 Biolegend). For proliferation analysis, mice were labeled for 24 h with one intraperitoneal injection of BrdU (50 mg/kg). After cell isolation, 25% of cells were fixed, stained, and analyzed for BrdU as described above.

Subcutaneous tumors were observed, and tumor size was measured at approximately 10 d after injection when tumors had volumes between 50 and 120 mm^3. The mice were randomly divided into two groups of equal tumor volume and injected intraperitoneally with 1 mg/kg KT-203 or DMSO (1% in 0.9% saline solution) once per day. Four to five mice were used per individual experiment per group. No blinding or exclusion criteria were applied. Mice were analyzed after 20 d of treatment. Mice that received KT-203 treatment were healthy and did not show any signs of treatment-associated toxicity, as observed by weight loss, overall appearance, and agility as well as macroscopic organ examination upon analysis.

No statistical method was used to predetermine sample size. All experiments were performed in accordance with Stanford University Animal Care and Use Committee guidelines.

Histology and immunohistochemistry. Lung samples were fixed in 4% formalin and paraffin embedded. Hematoxylin and eosin staining was performed using standard methods. Immunohistochemistry was performed using standard methods and standard antigen unmasking (1 mM citrate buffer, pH 6). Primary immunoblotting antibodies were against RFP (1:1,000 dilution, Rockland, 600-401-379), human nucleoli (1:500 dilution, Abcam, NM95), and BrdU (1:500 dilution, BD Biosciences, 3D4). Percent tumor area was calculated using ImageJ. Tomato$^+$ or BrdU$^+$ cells per optical field were counted using ImageJ on 10 randomly chosen 20× fields per section.

Statistics. Graphs and statistics were generated using the GraphPad Prism software. Significance, where indicated, was calculated using the two-sided Mann–Whitney test for nonparametric, unpaired data.

Synthetic schemes and compound characterization. Synthetic schemes and compound characterization are detailed in **Supplementary Note 1**.

45. Li, C.M. *et al.* Differential *Tks5* isoform expression contributes to metastatic invasion of lung adenocarcinoma. *Genes Dev.* **27**, 1557–1567 (2013).

46. Inloes, J.M. *et al.* The hereditary spastic paraplegia-related enzyme DDHD2 is a principal brain triglyceride lipase. *Proc. Natl. Acad. Sci. USA* **111**, 14924–14929 (2014).

47. Washburn, M.P., Wolters, D. & Yates, J.R. III. Large-scale analysis of the yeast proteome by multidimensional protein identification technology. *Nat. Biotechnol.* **19**, 242–247 (2001).

48. Weerapana, E. *et al.* Quantitative reactivity profiling predicts functional cysteines in proteomes. *Nature* **468**, 790–795 (2010).

49. Barretina, J. *et al.* The Cancer Cell Line Encyclopedia enables predictive modelling of anticancer drug sensitivity. *Nature* **483**, 603–607 (2012).